BioGecko

Vol 12 Issue 03 2023

ISSN NO: 2230-5807

Flow Characteristics of MHD Radiative Heat Absorbing/Generating Nanofluid with Variable Temperature

S. Venkata Ramireddy[1], K. Janardhan[2*], M. Umamaheswar[3], P. Chandra Reddy[4], V. Ravi Kumar[5]

[1]Associate Professor Department of Mathematics, School of Sciences MallaReddy University, Hyderabad, Telangana-500043

*[*2,3,4,5]Assistant Professor Department of Mathematics, Annamacharya Institute of Technology and Sciences, Rajampet, Kadapa (Dist.) Andhra Pradesh, India.*

**Corresponding Author Email: [2*]janardhankodidal@gmail.com*

Abstract

The effect of a nano MHD free convective radiation heat absorbing/generating viscous dissipative Newtonian fluid under variable temperature has been investigated in the current theoretical work. Using a numerical finite difference approach, the governing equations for the problem are resolved for velocity, temperature, and concentration. Graphs are used to study and depict the fluctuations in velocity, temperature, and concentration caused by the influence of various physical parameters. Additionally, we have noted the numbers for local skin friction, heat transfer, and mass transfer rates and talked about each one's features.

1. INTRODUCTION

In 1915, Oswald [1] used the term "nano" for the first time in his book "Te World of Neglected Dimensions." Because matter has a special characteristic at the nanoscale, nanotechnology is a popular research topic in the twenty-first century. Researchers and scientists from all over the world have been working continuously on various facets of nanotechnology in recent decades. The performance of heat transfer can be significantly enhanced by suspending metallic and nonmetallic particles in ordinary gases. The development of nanotechnology and related manufacturing methods has made it possible to create particles with a nanometer size. According to Choi S.U.S. [2], nanofuids are heat transfer fluids that contain nanomaterials (width less than 100 nm) to enhance the qualities of heat transmission. The ultimate goal of nanofluids is to maximise thermal conductivity with the fewest number of nanoparticles possible. Due to a nanofluid's improved thermal conductivity, it was able to cool microchannels without clogging and pump more effectively, among other benefits. Ahmad et al.'s [3] investigation of the nanofluid flow dynamics past a Riga plate used both analytical and numerical methods. They came to the conclusion that the size of the nanoparticles is proportional to the Nusselt number's magnitude. Using a computational method, Sheremet et al. [4] examined how the corner heater affected MHD nanofluid flow in a porous wavy cavity and demonstrated that the magnetic field has a detrimental effect on heat transmission. Sheikholeslami and Rokni [5] conducted a study on induced magnetic field impact on MHD between two parallel vertical plates with nanofluid and concluded that the temperature gradient of the nanofluid enhances with suction parameter augment but decreases with thermophoretic parameter augment. A thorough report on nanofluid forced convection flow in porous medium with a magnetic field was presented by Sheikholeslami et al. [6]. They came to the conclusion that Hartmann number causes a reduction in heat transport. Sheikholeslami [7] determined that

the radiation enhancement lowers the temperature gradient after numerically analysing the transport of MHD nanofluid flow in a permeable medium with radiation effect. The considerable impact of the ramp rate on the magnetic field in ferrofluid was examined by Vinod and Philip [8]. Their findings showed that as the magnetic field increased, the thermal conductivity increased as well.

2. MATHEMATICAL FORMULATION:

We consider an unsteady Nano_Magneto Hydrodynamics fluid radiation free convective heat absorbing/generating fluid with variable temperature in vertical channel. The x-axis is taken parallel to the channel, while the y-axis is taken perpendicular to it. The B_0uniform magnetic field applied to the flow in a transverse direction. When time $t \leq 0$ the fluid is at rest and the plate is kept at atemperature greater than the surrounding air temperatureT_∞. Temperature drops with temperature $T = \frac{1}{1+at}$ at time $t > 0$ and the plate exponential accelerates with increasing time in its own plane. The species concentration drops with time't' in a similar manner. It is presumpted that the effect of viscous dissipation is minimal and that the boundary layer and standard Boussineq's approximation will work. The flow is controlled by the following equations in light of the aforementioned factors.

$$\rho_{nf}\frac{\partial u^*}{\partial t^*} = \mu_{nf}\frac{\partial^2 u^*}{\partial t^{*2}} + g\rho\beta_{nf}(T^* - T_\infty) - \sigma_{nf}B_0^2 u^* - \frac{\mu_{nf}}{k^*}u^* \tag{1}$$

$$\rho C_{p_{nf}}\frac{\partial T^*}{\partial t^*} = K_{nf}\frac{\partial^2 u^*}{\partial t^{*2}} - \frac{\partial q_r^*}{\partial y^*} - Q^*(T^* - T_\infty) \tag{2}$$

The associated initial and boundary conditions of the illustrated model are as follows:

$$\left.\begin{array}{rl} t \leq 0 : u^* = 0\,,\ T^* = T_\infty\,, & for\ all \quad y^* \leq 0 \\ t > 0 : u^* = U_0 a^* t^*\,,\ T^* = T_\infty + \left(\frac{T_S^* - T_\infty}{1+At^*}\right), & at \quad y^* = 0 \\ u^* = 0\,, \qquad T^* = T_\infty\,, & as \quad y^* \to \infty \end{array}\right\} \tag{3}$$

Where $A = \frac{U_0^2}{\nu}$

Introducing the dimensionless variables and parameters are as follows:

$$\left.\begin{array}{c} U = \frac{u^*}{U_0}\,, y = \frac{y^* U_0}{\nu}\,, t = \frac{t^* U_0}{\nu}\,, \theta = \frac{T^* - T_\infty}{T_S^* - T_\infty}, a = \frac{a^*\nu}{U_0},\ K = \frac{k^* U_0^2}{\nu^2},\ \frac{\partial q_r^*}{\partial y^*} = 4(T^* - T_\infty)I^* \\ M^2 = \frac{B_0^2\sigma_f\nu_f}{\rho_f U_0^2}, G_r = \frac{g\beta_f\nu_f}{U^3}(T_S - T_\infty)\,, F = \frac{4\,I^*\nu_f}{\rho_f C_{p_f} U_0^2}\,, Q = \frac{Q^*\nu_f^2}{K_f U_0^2}, P_r = \frac{\nu_f\,\rho_f\,C_{p_f}}{K_f} \end{array}\right\} \tag{4}$$

We obtain the dimensionless governing system of partial differential equations of the model as follows:

$$a_1\frac{\partial U}{\partial t} = a_2\frac{\partial^2 U}{\partial y^2} - \left(a_3 M^2 + \frac{a_2}{K}\right)U + G_r a_4\theta \tag{5}$$

$$a_5\frac{\partial \theta}{\partial t} = \frac{a_6}{P_r}\frac{\partial^2\theta}{\partial y^2} - \left(F + \frac{Q}{P_r}\right)\theta \tag{6}$$

The analogous initial and boundary conditions becomes:

$$\left.\begin{array}{ll} t \le 0: & U = 0,\ \theta = 0,\quad for\ all \quad y \le 0 \\ t > 0: & U = at,\ \theta = \frac{1}{1+t},\quad at \quad y = 0 \\ & U = 0,\quad \theta = 0,\quad as\ \ y \to \infty \end{array}\right\} \qquad (7)$$

3. METHOD OF SOLUTION:

i. Numerical solution:

The finite difference approach has been introduced in order to solve the system of partial differential equations (5) and (6) with boundary conditions (7) mentioned above.

$$a_1\left(\frac{U_{i,j+1}-U_{i,j}}{\Delta t}\right) = a_2\left(\frac{U_{i-1,j}-2U_{i,j}+U_{i+1,j}}{(\Delta y)^2}\right) + a_4 G_r \theta_{i,j} - \left(a_3 M^2 + \frac{a_2}{K}\right) U_{i,j} \qquad (8)$$

$$a_5\left(\frac{\theta_{i,j+1}-\theta_{i,j}}{\Delta t}\right) = \frac{a_6}{P_r}\left(\frac{\theta_{i-1,j}-2\theta_{i,j}+\theta_{i+1,j}}{(\Delta y)^2}\right) - \left(F + \frac{Q}{P_r}\right)\theta_{i,j} \qquad (9)$$

Hear index *i* refer to y and *j* refers to time; the mesh system is divided by taking$\Delta y = 0.1$. From the initial conditions in (7) we have the following equivalent

$$\left.\begin{array}{l} U(0,j) = at, \theta(0,j) = \frac{1}{1+t}\ \ for\ all\ j \\ U(i_{max},j) = 0, \theta(i_{max},j) = 0\ for\ all\ j \end{array}\right\} \qquad (10)$$

(Here i_{max} was taken as 200), the velocity at the end of tie step viz, $\left(U_{i,j+1}\right)(i = 1, 200)$ is coupled form (8) in terms of velocity and temperature at point on the earlier time- step. After that $\left(\theta_{i,j+1}\right)$ is computed for (9). The procedure is repeated until $t = 0.5\ (i.e., j = 500)$, during the computation Δt was chosen as 0.001.

ii. Analytical solution:

The boundary conditions (7) around the fluid in the plate must be met in order to solve the system of partial differential equations (5) and (6) mentioned above.

$$\left.\begin{array}{l} U = U_0(y) + \varepsilon e^{at} U_1(y) \\ \theta = \theta_0(y) + \varepsilon e^{at} \theta_1(y) \end{array}\right\} \qquad (11)$$

Equating the harmonic and non-harmonic terms with (8) in equations (5) and (6), we get

Zeroth order equations:

$$U_0'' - \beta_2 U_0 = -\beta_5 \theta_0 \qquad (12)$$

$$\theta_0'' - \beta_4 \theta_0 = 0 \qquad (13)$$

First order equations:

$$U_1'' - \beta_3 U_1 = -\beta_6 \theta_1 \qquad (14)$$

$$\theta_1'' - \beta_1 \theta_1 = 0 \qquad (15)$$

The analogous boundary conditions become:

$$\left.\begin{array}{llll} U_0 = at\,,\ U_1 = 0, & \theta_0 = \frac{1}{1+t}\,,\ \theta_1 = 0 & at & y = 0 \\ U_0 \to 0\,,\ U_1 \to 0, & \theta_0 \to 0\,,\ \theta_1 \to 0 & as & y \to \infty \end{array}\right\} \quad (16)$$

Equations (12) through (15) are solved for under initial and boundary conditions (16), and the result is:

$$\theta_0 = L_1 e^{-y\sqrt{\beta_4}} \quad ; \quad \theta_1 = 0 \quad (17)$$

$$U_0 = L_3 e^{-y\sqrt{\beta_2}} + L_2 e^{-y\sqrt{\beta_4}} \quad ; \quad U_1 = 0 \quad (18)$$

Given the aforementioned equations, (11) can be expressed as:

$$\theta = L_1 e^{-y\sqrt{\beta_4}} \quad (19)$$

$$U = L_3 e^{-y\sqrt{\beta_2}} + L_2 e^{-y\sqrt{\beta_4}} \quad (20)$$

Skin friction coefficient:

$$\tau = \left(\frac{\partial U}{\partial y}\right)_{y=0} = -\left(\sqrt{\beta_2}\, L_3 + \sqrt{\beta_4}\, L_2\right) \quad (21)$$

Rate of heat transfer coefficient:

$$N_u = \left(\frac{\partial \theta}{\partial y}\right)_{y=0} = -\sqrt{\beta_4}\, L_1 \quad (22)$$

4. RESULTS AND DISCUSSION:

Numerical calculations are made for a variety of parameters, including $M,\ F, \emptyset, P_r, K,\ a, t$ velocity, temperature skin friction, and nusselt number, and the results are graphically displayed in Figures (1) through (12). The effects of the dimensionless solid volume fraction of nanoparticles parameter $\emptyset$ are shown in Figure 1. This graph demonstrates that velocity decreases as the dimensionless solid volume fraction of nanoparticles parameter.

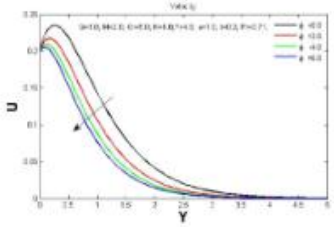

fig-1: velocity distributions for various values of

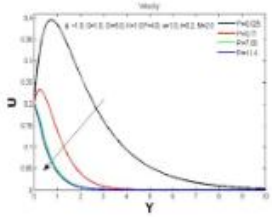

fig-2: velocity distributions for various values of

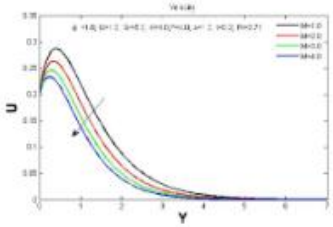

Fig-3: velocity distributions for various values of

The impact of the Prandtl number P_r on the velocity distribution is shown in Figure (2). It is observed that the velocity falls off as the Prandtl number $P_r$rises. This is due to the fact that low Prandtl number P_r fluids have high thermal diffusivity, which leads to greater temperatures in constant state. This, in turn, results in stronger buoyancy force, or higher fluid velocity, compared to fluids with relatively low Prandtl numbersP_r. In figure (3), the effect of the magnetic parameter M is depicted visually. The mean velocity drops as the magnetic parameter increases, as expected. The transverse magnetic field's influence produces a drag-like resistive type of force that tends to oppose the viscoelastic fluid's tendency to move more slowly.

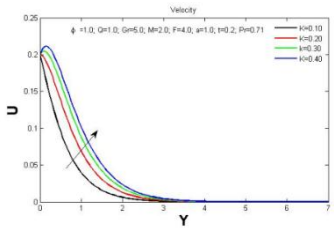

Fig-4: velocity distributions for various values of k

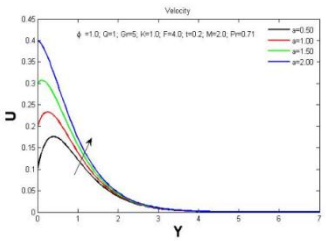

Fig-5: velocity distributions for various values of F

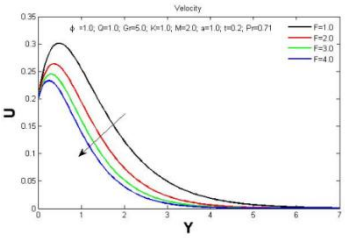

Fig-6: velocity distributions for various values of a

Figure (4) shows the fluctuation of velocity profiles with a dimensionless permeability parameter K. This graph unequivocally shows that as the dimensionless permeability parameter K is raised, the value of velocity profiles diminishes. The impact of the radiation parameter on the velocity distribution is shown in Figure (5). With rising radiation parameter values, it is shown that the velocity decreases. The velocity profiles for various values of the accelerating parameter "a" are shown in Figure (6). The figure shows that the velocity rises as the accelerating parameter rises. Additionally, it is discovered that the fluid velocity caused by an exponentially accelerated start (accelerating parameter not equal to zero) is greater than that caused by an impulsive start of the plate (accelerating parameter equal to zero).

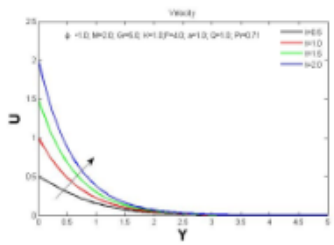

Fig-7: velocity distributions for various values of

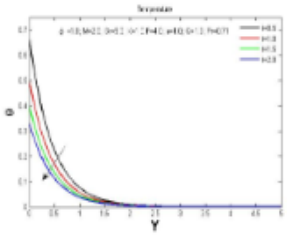

Fig-8: temperature distributions for various values of

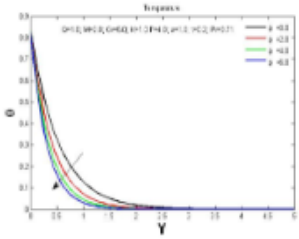

Fig-9: temperature distributions for various values of

The effects of the dimensionless time parameter "t" are seen in Figure (7). This graph shows that as the dimensionless time parameter is increased, velocity continues to climb. Figure (8) illustrates typical temperature profile fluctuation for various values of the dimensionless time parameter t. The findings demonstrate that a drop occurs as the dimensionless time parameter is increased. In the case of heat-absorbing fluids, the momentum and thermal boundary layers consequently get thinner.

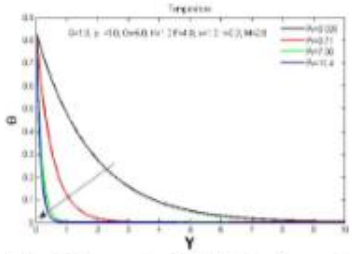

Fig-10: temperature distributions for various values of

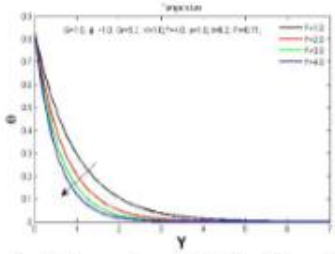

Fig-11: temperature distributions for various values of

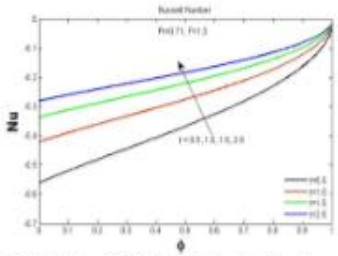

Fig-12: Rate of Heat transfere distributions for various values of

Figure (9) illustrates typical temperature profile fluctuation for various values of the dimensionless solid volume fraction of nanoparticles parameter ∅. The findings demonstrate

that a drop occurs as the dimensionless solid volume fraction of nanoparticles parameter Ø is increased. Figure (10) shows how the Prandtl number affects temperature. It is observed that when the Prandtl number rises, the surface temperature falls. This occurs because decreased fluid velocity prevents heat from convecting as easily, resulting in a drop in surface temperature. The impact of the radiation parameter on temperature distribution is seen in Figure (11). It demonstrates that as the radiation parameter's values rise, the temperature falls. The impact of the time parameter t on the Nusselt number is depicted in Figure (12). It is obvious that the Nusselt number rises as the value of the time parameter t grows.

5. REFERENCES

1. Oswald, W. *The world of neglected dimensions* (Dresden, Germany, 1915).
2. Choi, S. US, and Jeffrey A. Eastman. Enhancing thermal conductivity of fluids with nanoparticles. No. ANL/MSD/CP-84938; CONF-951135-29. Argonne National Lab.(ANL), Argonne, IL (United States), (1995).
3. Ahmad A, Asghar S, Afzal S (2016) Flow of nanofluid past a Riga plate. J Magn Magn Mater 402:44–48.
4. Sheremet MA, Oztop HF, Pop I (2016) MHD natural convection in an inclined wavy cavity with corner heater filled with a nanofluid. J Magn Magn Mater 416:37–47.
5. Sheikholeslami M, Rokni HB (2017) Nanofluid two phase model analysis in existence of induced magnetic field. Int J Heat Mass Transf 107:288–299
6. Sheikholeslami M, Shehzad SA, Abbasi FM, Li Z (2018) Nanofluid flow and forced convection heat transfer due to Lorentz forces in a porous lid driven cubic enclosure with hot obstacle. Comput Methods Appl Mech Eng 338:491–505.
7. Sheikholeslami M (2019) Numerical approach for MHD Al2O3-water nanofluid transportation inside a permeable medium using innovative computer method. Comput Methods Appl Mech Eng 344:306–318
8. Vinod S, Philip J (2020) Impact of field ramp rate on magnetic field assisted thermal transport in ferrofluids. J Mol Liq 298:112047.